Stereo Accuracy for Collision Avoidance for Non-linear Collision Trajectories

Waqar Khan and Reinhard Klette

***Abstract*— In this study, we have generalized our previous tool for assisting a safety engineer in assessing collision trajectories by extending from colliding objects with constant velocity to more general variable velocity ones. We have also highlighted that a linear system cannot be relied upon for handling a colliding object with variable velocity. To deal with such trajectories, past observations are weighted depending on velocities at those locations; priority is given to locations with reduced velocity. Based on this hypothesis, we have shown that the weighted system outperforms a linear one. The benefit is that it always issues a timely warning, even if the trajectory of the colliding object keeps on changing over time.**

I. INTRODUCTION

Stereo vision faces similar limitations as various other computer science applications - an improvement has a certain cost. Accuracy of stereo improves by increasing image resolution but at the cost of an increased disparity range. This range is proportional to the memory required for a real-time (yet accurate) hardware implementation of a stereo matching algorithm like *Dynamic Programming* stereo (DP), *Semi-Global Matching* stereo (SGM), *Belief Propagation* stereo (BP) [10], or *Graph Cut* stereo (GC); see, for example, [4], [7], [13], [17]. For example, memory needed for BP is $\mathcal{O}(MNd_{max})$ [15], for images of size $M \times N$ and d_{max} disparity levels.

If the image resolution is increased, the camera sensor captures more detail in the scene but the sensor still contains discrete pixels, hence the disparity values are still integral. Accordingly, the depth is measured at discrete steps [12]. Stereo matching algorithms often generate sub-pixel disparities, but still the disparities remain a discrete representation of a continuous world. In other words, for every measured depth, there is an inherent inaccuracy involved. In a controlled environment with known location of the object of interest, this stereo limitation is significantly reduced by an appropriate off-line stereo configuration. However, when the locations of objects of interest are unknown as in the case of dynamic stereo imaging, then determining the accuracy of estimated depth (or trajectory) becomes an interesting problem.

In stereo photogrammetry, the depth resolution is better at close distance than for objects farther away. So, with an object approaching an *ego-vehicle* (i.e., the vehicle the stereo system is operating in), the accuracy of the estimated trajectory would appear to improve over time, allowing for better estimates of the possibility of a collision scenario [11], [6]. Due to the integral measurable depths, the stereo system installed on an ego-vehicle for driver assistance, will have some uncertainties for estimating an object trajectory and issuing a warning [8]. Timing of the warning and its accuracy are crucial for setting the confidence of a driver over the system. An earlier accurate warning improves the driver's confidence over the system, whereas false or late warnings degrade this confidence [1], [2]. For a collision scenario, an accurate and timely warning issued by the safety system is a challenge.

As highlighted previously [9], for a collision scenario with a colliding object moving with constant velocity, a stereo-based safety system can issue timely warnings. However, due to the uncertainties in estimated trajectories, warnings can also be false. Here, we generalize the previously used model further by considering an object moving with constant speed but variable direction.

W. Khan and R. Klette are with the Computer Science Department, Tamaki Innovation Campus, The University of Auckland, New Zealand. Contact email: wkha011@aucklanduni.ac.nz

II. ASSUMPTIONS

A **colliding object** is rigid and is of size $L \times W \times H$, and is travelling with constant speed V on a flat surface with $Y = 0$, however its direction of motion may vary along XZ-components over time. The object's L dimension is always in the direction of the object's motion. The colliding object first appears at $\overrightarrow{O(0)} = [O_x(0), O_y(0), O_z(0)]^T$. As the direction of motion changes, the pose of the object will change accordingly.

The **ego-vehicle** starts at $\overrightarrow{O^i(0)} = \left[O_x^i(0), O_y^i(0), O_z^i(0)\right]^T$ and travels at a constant velocity $\overrightarrow{V^i}$ in the direction of the Z-axis so that $O_x^i = V_x^i = O_y^i = V_y^i = 0$. We define an exclusion zone around the ego-vehicle of radius r_{exc}.

At frame 0, n equidistant and binocularly visible **feature points** are chosen over the extent of an object. The closest of them is the reference point for the object.

A. Single vs. More Feature Points

In object tracking, an object is often referred to as by a single reference point. However, when the pose of an object is changing, as is here, then the single reference point may observe the change in object position later than closer feature points. This is particularly important when the extent of object covers more than one disparity values.

Figure II-A shows an example scenario. In this scenario, a toy-car of dimensions $[L \times W \times H] = [0.1, 0.1, 0.3]\,m$ is rotating around its XZ-centre. We use a stereo system in canonical configuration, defined by parameters $f = 16mm$, $b = 60mm$, $\delta s = 0.03s$ and $\tau = 4.65\mu m$. The stereo

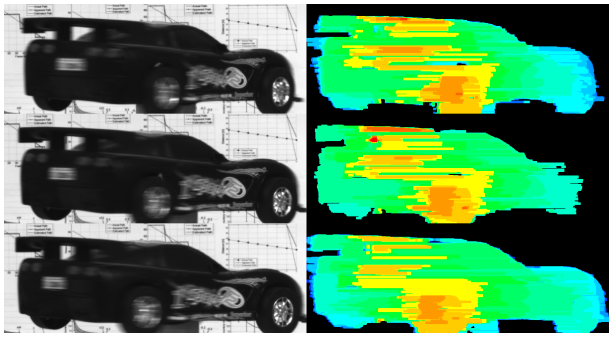

Fig. 1. Left column shows the left camera images, and the right column shows the colour-coded disparities (the streaking effects are due to a used DP matcher) after background subtraction. Pose of the car is changing clockwise while observed from Y-axis (top).

system uses a DP matcher [14] to generate dense disparity maps at each pixel (no sub-pixel accuracy). After background subtraction, we colour-code the disparity levels over the extent of the toy-car.

As the pose of the toy-car changes over time, the observed disparities over the toy-car's surface also change accordingly. Due to non-linear uncertainties, only few pixels over the surface are observed at a different disparity in δs. Therefore, instead of using a single feature point, multiple feature points can assist in improving the system's decision.

As common for a safety system, the nearest object position is considered to safely avoid the worst case scenario. For the sequence used in Figure II-A with some post-processing, the nearest feature point can be chosen as a top-corner point, central point, or a bottom-corner point. Post-processing involves excluding smaller real-world contours on the toy-car, i.e. smaller than $[L \times W \times H] = [0, 0.10, 0.05]\, m$.

The output is the measured distance of each chosen feature point from the centre of the baseline over time, and is shown in Figure II-A. The distance of each point with respect to the other is quite similar apart from the few occasions where a DP mismatch occurs. (So, to handle mismatches, it would also be good to use more than one feature point to vote for the best outcome; but we do not do so in our experiments.)

III. ALWAYS COLLIDING TRAJECTORY

From the ego-vehicle's point of reference $\overrightarrow{C} = [0, 0, 0]^T$, an object represented by a single reference point is first observed

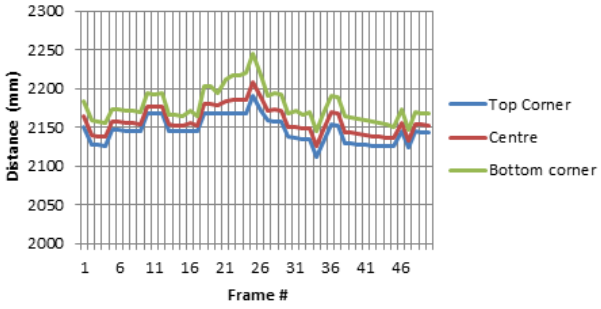

Fig. 2. Distance of three nearest points on the toy-car from the centre of the baseline.

$(k = 0)$ at position $\overrightarrow{O^r(k)} = \left[O_x^r(k), O_y^r(k), O_z^r(k)\right]^T$ at distance D_k^r and is moving with constant speed V^r (see Figure III). Superscript r denotes the computations made in ego-vehicle's point of reference.

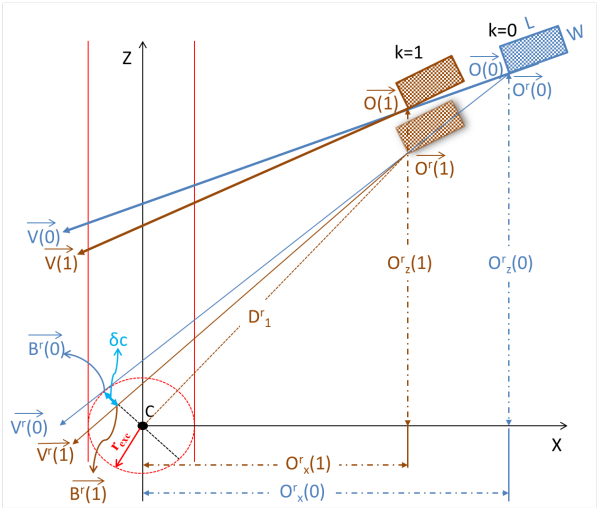

Fig. 3. Object velocity changes with each observation. For an always colliding object, the object crosses the exclusion zone of radius r_{exc}. See the text for further explanations.

The object is initially on a collision course ζ_k^r as a left tangent $\zeta_L^r = tan^{-1}\left(\frac{-O_z^r(k)}{-O_x^r(k)}\right) - sin^{-1}\left(\frac{r_{exc}}{D^r(k)}\right)$ to the ego-vehicle's exclusion zone. Where, $D^r(k) = \sqrt{(O_x^r(k))^2 + (O_z^r(k))^2}$ is the distance of object from the ego-vehicle. Note that angles ζ_L^r and ζ_k^r are in polar coordinates.

The initial object velocity equals

$$\overrightarrow{V^r(k)} = \begin{bmatrix} V^r \cos\zeta_k^r \\ 0 \\ V^r \sin\zeta_k^r \end{bmatrix} \quad (1)$$

with object's L dimension in the direction of $\overrightarrow{V(k)}$. After each system observation $k-1$, the object moves to a new position $\overrightarrow{O^r(k)} = \overrightarrow{O^r(k-1)} + (\overrightarrow{V^r(k-1)} \cdot \delta s)$. The model assumes that object changes its trajectory after every observation too. This effectively would also change object pose, derived by repositioning n feature points (see Section IV). The object trajectory changes from ζ_{k-1}^r to $\zeta_{k-1}^r \pm \delta c$, where δc is the *rate of change of angular velocity* and is input to the model (see Figure III).

Notation $\pm$ can either be $+$ or $-$. Figure 4 illustrates the use of the $\pm$ notation. The same procedure is also later explained in Algorithm 1. At $k = 0$, labelled as position A in Figure 4, object trajectory $\zeta_0^r = \zeta_L^r$. For the following observations, $\pm = +$ is used by the model, to change object trajectories from A to C. Later, if $\pm = +$ is used any further, then $(\zeta_{k-1}^r + \delta c) > \zeta_R^r$, where $\zeta_R^r = tan^{-1}\left(\frac{-O_z^r(k)}{-O_x^r(k)}\right) + sin^{-1}\left(\frac{r_{exc}}{D^r(k)}\right)$ is the right tangent to the ego-vehicle exclusion zone from the object at observation k. At this trajectory, the object would pass behind the ego-vehicle. So, for a collision scenario, $\pm = -$ is used for trajectories between C and E.

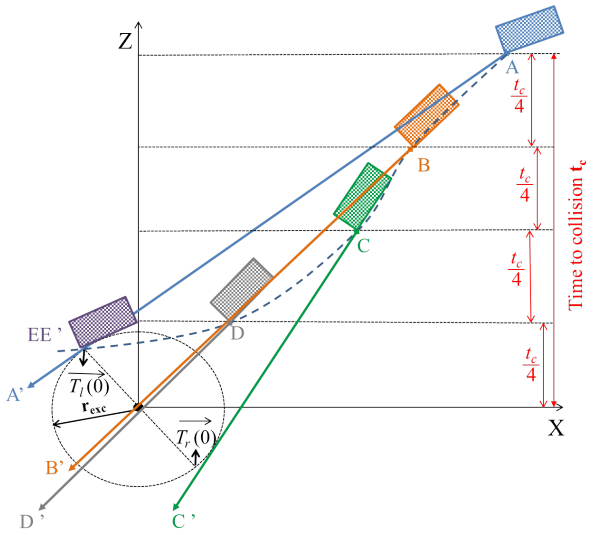

Fig. 4. The trajectory of an object varies with each observation k. Four example, trajectories A, B, C and D are shown in relative frames of reference. The pose of the object at each instance is different relative to the ego-vehicle. The object covers the collision path in t_c seconds.

IV. OBJECT POSE

The pose of an object is determined based on its real-world velocity derived from $\overrightarrow{V^r(k)}$ as in Equation 1, defined by

$$\overrightarrow{V(k)} = \begin{bmatrix} V_x^r(k) \\ 0 \\ V_z^r(k) + V_z^i \end{bmatrix} \tag{2}$$

The angle of the actual object trajectory, relative to the X-axis, is $\eta_k = tan^{-1}(\frac{V_z(k)}{V_x(k)})$, and it is used by the model to determine the object pose before observation k (and after system observation $k-1$).

In the model, we consider n equidistant feature points on the surface of the colliding object. The nearest observed point in real-world coordinates is the reference point $\overrightarrow{O_j(k)}$ (at $j=1$), and it is at position $\overrightarrow{O^r(k)}$.

As the object trajectory changes with respect to $\overrightarrow{V(k)}$, η_k also changes. This leads to a change in positions of each feature point on the object's surface with respect to the object reference point $\overrightarrow{O_1(k)}$.

The feature point j at distance c from $\overrightarrow{O_1(k)}$ along the W dimension moves to

$$\overrightarrow{O_j(k)} = \begin{bmatrix} O_{1x}(k) + c\cos\left(\eta_k - \frac{\pi}{2}\right) \\ 0 \\ O_{1z}(k) + c\sin\left(\eta_k - \frac{\pi}{2}\right) \end{bmatrix} \tag{3}$$

Similarly, the feature point j at distance c from $\overrightarrow{O_1(k)}$ along the L dimension moves to

$$\overrightarrow{O_j(k)} = \begin{bmatrix} O_{1x}(k) + c\cos\left(\eta_k - \pi\right) \\ 0 \\ O_{1z}(k) + c\sin\left(\eta_k - \pi\right) \end{bmatrix} \tag{4}$$

It is assumed that the system makes observation k, after, the object pose has been pre-adjusted by the model. Algorithm 1

GeneralCollisionTrajectories$(\delta s, V^r, \delta c, r_{exc}, \overrightarrow{V^i}, \overrightarrow{O(0)})$
returns system state **S** at each observation k;
Initialize state, **S** $\leftarrow$ **S0** and observations $k = -1$;
Object initial relative position $\overrightarrow{O^r(0)} = \overrightarrow{O(0)}$;

for each observation k **do**
  Relative object distance $D^r(k) = \|\overrightarrow{O^r(k)}\|$;
  Relative collision trajectory to the ego-vehicle is $\zeta_k = tan^{-1}\left(\frac{-O_z^r(k)}{-O_x^r(k)}\right)$;
  Left tangent to exclusion zone in polar coordinates is $\zeta_L^r = \zeta_k - sin^{-1}\left(\frac{r_{exc}}{D^r(k)}\right)$;
  Right tangent to exclusion zone in polar coordinates is $\zeta_L^r = \zeta_k + sin^{-1}\left(\frac{r_{exc}}{D^r(k)}\right)$;
  if First observation at $k=0$ **then**
    Initial collision trajectory is the left tangent, $\zeta_k^r = \zeta_L^r$;
    For $\pm$ notation **SET** $MinusFlag \leftarrow TRUE$;
  else
    if ζ_k^r is supposed to increase $(MinusFlag == FALSE)$ **then**
      if $\left(\zeta_{k-1}^r + \delta c\right) > \zeta_R^r$ **then**
        ζ_k^r has to decrease, **SET** $MinusFlag \leftarrow TRUE$;
      else
        ζ_k^r has to increase, **SET** $MinusFlag \leftarrow FALSE$;
      end if
    else
      if $\left(\zeta_{k-1}^r + \delta c\right) < \zeta_L^r$ **then**
        ζ_k^r has to increase, **SET** $MinusFlag \leftarrow FALSE$;
      else
        ζ_k^r has to decrease, **SET** $MinusFlag \leftarrow TRUE$;
      end if
    end if
  end if
  if $MinusFlag == TRUE$ **then**
    Decrease $\zeta_k^r = \zeta_{k-1}^r - \delta c$;
  else
    Increase $\zeta_k^r = \zeta_{k-1}^r + \delta c$;
  end if
  Use Equation 1 to derive the relative object collision velocity $\overrightarrow{V^r(k)}$ at observation k;
  Use Section IV to determine the pose of the object;
  Use either the variable velocities in Section V-A to determine the system state **S**;
  Before the next observation, the object moves to new position $\overrightarrow{O^r(k)} = \overrightarrow{O^r(k)} + \delta s\overrightarrow{V^r(k)}$;
end for

Fig. 5. Algorithm 1, modelling a collision scenario with variable velocity and decision making.

(see Fig. 5) shows the steps followed by the model to change object velocity and its pose before each system observation.

V. STEREO-BASED DRIVER ASSISTANCE SYSTEM

This model has the same design constraints as discussed in Section II. D. of [9]. Therefore, due to discrete disparities, the stereo measurements have uncertainty in them. This leads to a possible range of trajectories derived from the range ($\overrightarrow{min_j V^r}$ to $\overrightarrow{max_j V^r}$) of velocities (see Equations 10 and 11 of [9]). To handle the changing trajectories of an object travelling with variable velocity, we compute the weighted average of velocity ranges. This average is computed by first affiliating a weight $\overrightarrow{w^k} = \left[w_x^k, 0, w_z^k\right]^T$ to each feature point at observation k.

A. Weighted System

For simplicity, we assume that the following procedure would be applicable to each feature point. We also assume that the maximum legally permitted speed in a traffic scenario is V_{limit}. So, to handle the unrealistically high speed for the considered traffic scenario, the system assumes that the object speed would not exceed $V_{max} = sV_{limit}$, where s is the *speeding factor*. Parameter s is input to the model.

At observation k, weight $\overrightarrow{w^k}$ is directly related to the time $\overrightarrow{\Delta t}$ for which a feature point is observed at the same position (u, d) with some uncertainty $(\pm\nu_u, \pm\nu_d)$. $\overrightarrow{w^k}$ is also indirectly related to the uncertainty at the measured position $(\Delta X(u,d), \Delta Z(d))$,

$$\overrightarrow{w^k} = \begin{bmatrix} \frac{\Delta t_x}{\left|\widehat{X}^r_{1,k} - \widehat{X}^r_{0,k}\right|} \\ 0 \\ \frac{\Delta t_z \widehat{Z}^r_k}{\left|\widehat{Z}^r_{1,k} - \widehat{Z}^r_{0,k}\right|} \end{bmatrix} \tag{5}$$

where $\widehat{Z}^r_k$ is the observed $Z-$position at $\widehat{Z}^r = (u, d)$ at observation k. Similarly, $\widehat{X}^r_{0,k}$, $\widehat{X}^r_{1,k}$, $\widehat{Z}^r_{0,k}$, and $\widehat{Z}^r_{1,k}$ are the observed positions at the boundary of the measured pixel $\widehat{X}^r = (u + \nu_u, d - \nu_d)$, $\widehat{X}^r = (u - \nu_u, d + \nu_d)$, $\widehat{Z}^r = (u, d - \nu_d)$, and $\widehat{Z}^r = (u, d + \nu_d)$. $\widehat{Z}^r_k$ is used in Equation 5 as a scaling factor for the $Z-$term of $\overrightarrow{w^k}$.

Due to the uncertainty of stereo measurement, the measured velocity is a range as already discussed in Equations 10 and 11 of [9]. To compute their weighted outcome at observation k, we generalize the measured velocity term as $\overrightarrow{mV^k}$. While, $\overrightarrow{wmV^k}$ as their corresponding weighted velocity,

$$\overrightarrow{wmV^k} = \begin{bmatrix} \frac{wV_x^{k-1}\sum_{i=0}^{k-1} w_x^i + mV_x^k \sum_{i=0}^{k} w_x^i}{\sum_{i=0}^{k-1} w_x^i + \sum_{i=0}^{k} w_x^i} \\ 0 \\ \frac{wV_z^{k-1}\sum_{i=0}^{k-1} w_z^i + mV_z^k \sum_{i=0}^{k} w_z^i}{\sum_{i=0}^{k-1} w_z^i + \sum_{i=0}^{k} w_z^i} \end{bmatrix} \tag{6}$$

where $\overrightarrow{wV^{k-1}}$ keeps the feedback from previous observations and is computed at previous observation $k-1$,

$$\overrightarrow{wV^k} = \begin{bmatrix} \frac{wV_x^{k-1}\sum_{i=0}^{k-1} w_x^i + mV_x^k w_x^k}{\sum_{i=0}^{k} w_x^i} \\ 0 \\ \frac{wV_z^{k-1}\sum_{i=0}^{k-1} w_z^i + mV_z^k w_z^k}{\sum_{i=0}^{k} w_z^i} \end{bmatrix} \tag{7}$$

At $k = 0$, we have that $\overrightarrow{wV^{k=0}} = \overrightarrow{mV^{k=0}}$ and $\overrightarrow{wmV^{k=0}} = \overrightarrow{mV^{k=0}} = 0$.

Velocity Extrema: For each feature point j, the velocity extrema (before weighted average) range between $\overrightarrow{min_j V^r}$ (see Equation 10 of [9]) and $\overrightarrow{max_j V^r}$ (see Equation 11 of [9]). Whereas, after weighted average using Equation 6, the weighted velocity extrema range between $\overrightarrow{minwm_j^k V^r}$ and $\overrightarrow{maxwm_j^k V^r}$.

Previously, the object was assumed to be moving with constant velocity and the system computed the velocity extrema to be the maximum values consistent with all previous observations. Here, however, since the object is moving with variable velocity, therefore the system chooses the best outcome based on the weight derived in Equation 7.

The object is still assumed to be rigid. Therefore, the system computes the largest minimum and the smallest maximum as a range of velocities being consistent with all feature point observations. Thus, for the whole object we have that

$$\overrightarrow{maxV^r} = \begin{bmatrix} min\left(maxwm_1^k V_x^r, \ldots, maxwm_n^k V_x^r\right) \\ 0 \\ min\left(maxwm_1^k V_z^r, \ldots, maxwm_n^k V_z^r\right) \end{bmatrix} \tag{8}$$

$$\overrightarrow{minV^r} = \begin{bmatrix} max\left(minwm_1^k V_x^r, \ldots, minwm_n^k V_x^r\right) \\ 0 \\ max\left(minwm_1^k V_z^r, \ldots, minwm_n^k V_z^r\right) \end{bmatrix} \tag{9}$$

The range of trajectory angles, (ρ_L,ρ_R), is then computed from the truncated $\overrightarrow{minV^r}$ and $\overrightarrow{maxV^r}$.

In order to judge a collision, the system follows the same procedures as in [9], Sections II.E.2, II.E.3, and II.E.4. Algorithm 1 of [9] becomes slightly different for modelling the motion of feature point(s) position based on Equation 3 and Equation 4 instead of $\overrightarrow{O^r_{k,j}} = \overrightarrow{O^r_{0,j}} + \overrightarrow{V^r}t$.

Over the course of time the system stays at one of the following states. **S0** for first observation, **S1** if object object is safe, **S2** if system uncertain of object course and can safely wait for another observation, **S3** if system uncertain of object course and not safe to wait for additional observations, or **S4** if object is on a collision course. For cases **S3** and **S4** system issues a braking warning.

VI. RESULTS AND DISCUSSION

The model has a wide range of parameters. We use the standard parameters from Table I. We assume that the disparity

TABLE I

SYSTEM PARAMETERS USED IN THE MODEL

Symbol	Description	Typical value
f	Focal length	$9\ mm$
τ	Pixel size	$4.7\ \mu m$
b	Baseline length	$750\ mm$
d_{max}	Maximum disparity	127
ϕ	Vergence angle	0°
δs	Sampling interval	$0.03\ s$
r_{exc}	Radius of vehicle's exclusion zone	$2\ m$
V^i	Vehicle speed	$17\ ms^{-1}$(60 kmh)
V^i_{crit}	Maximum collision speed	$2.77\ ms^{-1}$(10 kmh) [18]
V_{limit}	Maximum speed limit	$17\ ms^{-1}$(60 kmh)
s	Speeding factor	1.5
t_d	Driver response time	$0.5\ s$ [2], [3]
μ	Coefficient of friction	0.4 [16], [5]
t_p	Object detection and classification time	$1.5\ ms$
$(L \times H \times W)$	Object size	
δ_c	Rate of collision angle	0.1°
n	Maximum number of feature points	9
Derived Values		
V_{max}	Object maximum speed	$25.5\ ms^{-1}$ (90 kmh)
$Z_{min}(d_{max})$	Minimum depth in CFoV	$11.3\ m$
θ	Half angle of stereo field-of-view	14.9°
t_b	Vehicle braking time	$1.8\ s$ ([16])
D_b	Maximum safe braking distance	$44.4\ m$
Glossary		
ρ_L, ρ_R	Range of trajectory angles for an object	
ζ_L, ζ_R	Trajectory angles with (or tangents to) vehicle's exclusion zone	

map is with sub-pixel accuracy of up to two sub-pixels on a pixel.

In our previous study of linear systems, we highlighted that a stereo-based safety system is prone to issuing too many precautionary warnings. We also used two hypotheses to avoid generating the precautionary warnings when possible. Firstly, estimated high speeds were truncated to be not faster than V_{max}. Secondly, the system assumed that the object trajectory is constant and estimated the range of trajectories as being consistent with all the previous observations.

For objects approaching from farther locations, these hypotheses permitted the system to consider more observations before issuing a precautionary or necessary warning. However, now with more general collision trajectories, the second hypothesis may mislead the system in estimating a trajectory which was only initially true.

A. Experiment 1a: Linear vs. Weighted

Using the typical parameters from Table I, with $n = 1$, Figure 6(a) and Figure 6(b) shows the maximum tolerable speeds of a linear and a weighted system. The tolerable speeds are only for a collision scenario for objects first appearing at any of these locations within stereo CFoV.

In Figure 6, a weighted system outperforms a linear one. Both systems have similar behaviour at closer distances as both issue timely precautionary warnings. However at farther distances, while the object takes more time in colliding with the ego-vehicle, the system can safely delay the precautionary warning. More time should permit systems to improve their estimates. But, as the trajectory keeps changing, the linear system estimates that the object is safely avoiding the ego-vehicle. So, it fails to recognize a collision scenario. Whereas, the weighted system, gives weight to each measurement based on the time it is observed at the same location, hence avoids such false estimates.

B. Experiment 1b: Anomalies of a Linear System

For the typical system with Table I configuration parameters, a linear system shows certain anomalies at farther distances (see Figure 6(a)). To analyse these anomalies we assume two similar sized objects first appearing at two different locations **A**$= [4, 112]^T\ m$ and **B**$= [4, 114]^T\ m$ from the ego-vehicle. **A** being closer should have lower tolerable speed than **B**, however, the maximum tolerable speed of **A** (25.4 ms^{-1}) is unexpectedly higher than that of **B** (1.1 ms^{-1}). To analyse this anomaly, we consider the collision speed of $V = 1.2$ ms^{-1}intolerable by **B** but tolerable by **A**.

A being closer is first observed at $d = 13.5$, while **B** being farther away is first observed at $d = 13.0$ (sub-pixel level). After the 2nd observation, the system can determine the range of trajectories for the first time. At this stage, the system estimates that the objects could possibly collide, but as the objects are quite far from the ego-vehicle, so the system can safely wait for additional observations. After 61 observations for **A** with the object at $(2.6, 76.6)m$, the system can no longer wait for additional observations and hence issues a timely precautionary warning. Whereas, **B** is farther away at $(2.7, 78.6)m$ from ego-vehicle, thus the system chooses to consider additional observations. After observation 64 for **B**, the system has the estimated range of trajectories $(\rho_L, \rho_R) = (262.9, 266.8)^\circ$. As, this range is not crossing the ego-vehicle's exclusion zone tangents $(\zeta_L, \zeta_R) = (266.9, 269.9)^\circ$, so the system *falsely* estimates that **B** is safe.

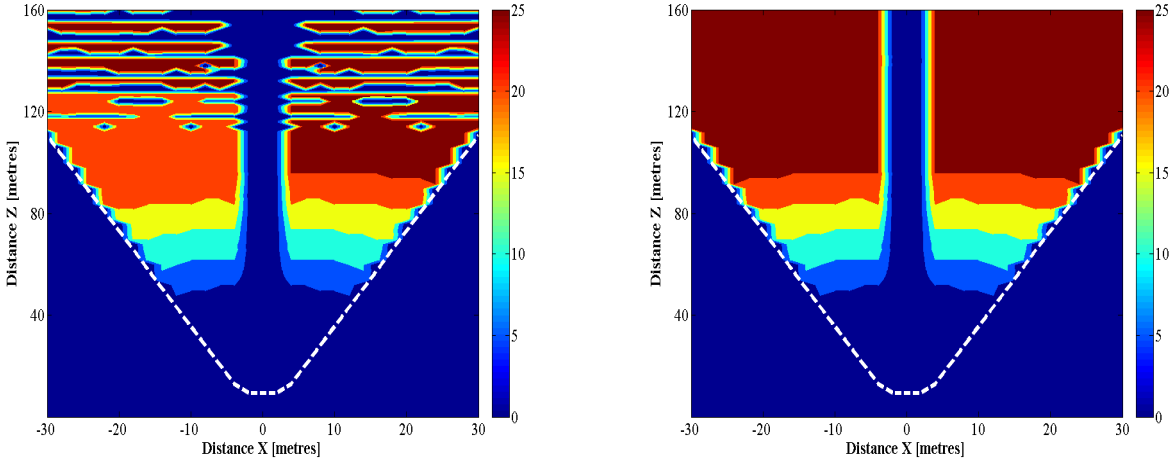

(a) Linear system: $b = 750mm$, $f = 9mm$, $\tau = 4.7\mu m$, $w \times h = 1024 \times 768$ pixels and $n = 1$

(b) Weighted system: $b = 750mm$, $f = 9mm$, $\tau = 4.7\mu m$, $w \times h = 1024 \times 768$ pixels and $n = 1$

Fig. 6. Tolerable speeds of linear and weighted systems for a collision scenario. Parameters not specified in captions are taken from Table I configuration parameters. The grey region within stereo CFoVhas tolerable speeds less than or equal to $V^i_{crit} = 2.7\ ms^{-1}$.

VII. CONCLUSIONS

The designed tool can assist a safety engineer in assessing the effect of various stereo configurations, and of vehicle and object parameters. Previously we designed a similar tool for constant object trajectories only. Now, modelling variable collision trajectories, we have shown that a linear system can falsely estimate a safe travel.

To mitigate this problem, we designed a weighted system which always issues a timely warning for a collision scenario - provided the object is binocularly visible CFoV. Although these warnings are timely, mostly they are precautionary as well, as the system is mostly unsure about the exact object trajectory to some extent, thus issuing a warning based on a *possible* worst case trajectory.

REFERENCES

[1] A. Genya, and J. H. Richardson. The influence of alarm timing on braking response and driver trust in low speed driving. *J. Safety Science*, pages 639–654, 2005.

[2] A. Genya, and J. H. Richardson. The influence of alarm timing on driver response to collision warning systems following system failure. *J. Behaviour & Information Technology*, pages 443–452, 2006.

[3] R. E. Dewar, P. L. Olson, and G. J Alexander. Human factors in traffic safety, 2002.

[4] P. F. Felzenszwalb, and D. P. Huttenlocher. Efficient belief propagation for early vision. *Int. J. of Computer Vision*, vol. 70, pages 41–54, 2006.

[5] D. E. Fume, and I. A. Sultan. A novel in-vehicle real-time brake-monitoring system. *J. Automobile Engineering*, vol. 223, pages 793–804, 2009.

[6] S. B.Goldberg, N. W. Maimone, L. Matthies, I. Syst, and C. A. Northridge. In Proc. *IEEE Proc. Aerospace Conf.*, vol. 5, 2002.

[7] S. Hermann and R. Klette. Iterative semi-global matching for robust driver assistance systems. In Proc. *Asian Conf. Computer Vision*, LNCS, 2012.

[8] W. Khan, J. Morris, and R. Klette. Stereo accuracy for collision avoidance. In Proc. *Int. Conf. Image Vision Computing New Zealand*, pages 67–72, 2009.

[9] W. Khan, and J. Morris. Safety of stereo driver assistance systems. In Proc. *IEEE Int. Vehicle Symp. (IV)*, pages 469–475, 2012 (see also `www.mi.auckland.ac.nz/tech-reports/MItech-TR-79.pdf`).

[10] W. Khan, V. Suaste, D. Caudillo, and R. Klette. Belief propagation stereo matching compared to iSGM on binocular or trinocular video data. In Proc. *IEEE Int. Vehicle Symp. (IV)*, 2013 (see also `http://www.mi.auckland.ac.nz/tech-reports/MItech-TR-82.pdf`).

[11] D. J. Kriegman, E. Triendl, and T. O. Binford. Stereo vision and navigation in buildings for mobile robots. *IEEE Trans. Robotics Automation*, vol. 5, pages 792–803, 1989.

[12] L. Matthies, and S. Shafer. Error modeling in stereo navigation. *IEEE J. Robotics Automation*, vol. 3, pages 239–248, 1987.

[13] S. Morales, J. Penc, T. Vaudrey, and R. Klette. Graph-cut versus belief-propagation stereo on real-world images. In Proc. *Iberoamerican Conf. Pattern Recognition*, LNCS 5856, pages 732-740, 2009.

[14] J. Morris, K. Jawed, and G. Gimel'farb. Intelligent Vision: A first step - real time stereovision. In Proc. *Int. Conf. Advanced Concepts Intell. Vision Systems*, LNCS 5807, pages 355–366, 2009.

[15] S. Park, and H. Jeong. A high-speed parallel architecture for stereo matching. In Proc. *Advances Visual Computing*, LNCS 4291, pages 334–342, 2006.

[16] A. Tang, and A. Yip. Collision avoidance timing analysis of DSRC-based vehicles. *J. Accident Analysis Prevention*, vol. 22, pages 182–195, 2010.

[17] M. Tappen, and W. Freeman. Comparison of graph cuts with belief propagation for stereo, using identical MRF parameters. In Proc. *IEEE Int. Conf. Computer Vision*, pages 900–906, 2003.

[18] P. Wramborg. A new approach to a safe and sustainable road structure and street design for urban areas. In Proc. *Road Safety Four Continents Conf.*, 2005.